Vagal Signaling Decline in Age-related Macular Degeneration Drives Spleen-Dependent Retinal Inflammation

Kaitryn E. Ronning[1*], Christophe Roubeix[1*], Caroline Nous[2], Sébastien Augustin[1], Frédéric Blond[1], Foteini Argyriou[1], Christopher Rue Molbech[3,4], Katalin Veres[5], Jesper Mehlsen[6], Marie Bak[7], Emmanuel L. Gautier[8], Henrik Toft Sørensen[5], Xavier Guillonneau[1%], Cécile Delarasse[1%], Torben Lykke Sørensen[3,4,%], Florian Sennlaub[1,2,%,†]

[1]Sorbonne University, INSERM, CNRS, Institut de la Vision, 17 rue Moreau, F-75012 Paris, France

[2]Centre Hospitalier National d'Ophtalmologie des Quinze-Vingts, INSERM-DHOS CIC 503, Paris, France

[3]Clinical Research Division, Department of Ophthalmology, Zealand University Hospital, Roskilde, Denmark

[4]Faculty of Health Sciences, University of Copenhagen, Denmark

[5]Department of Clinical Epidemiology and Center for Population Medicine, Aarhus University Hospital and Aarhus University, Denmark

[6]Department of Clinical Medicine, Rigshopitalet, Denmark

[7]Department of Haematology, Zealand University Hospital, Denmark

[8]Sorbonne University, Inserm, Nutrition and Obesity : Systemic Approaches, F-75013 Paris, France

%, * contributed equally

[†] Correspondence should be addressed to Dr Florian Sennlaub, INSERM, UMR_S 968, Institut de la Vision, Paris, F-75012, France. Tel: (33) 1 53 46 26 93, Email: florian.sennlaub@inserm.fr

Abstract

Under relaxed physiological conditions, vagal innervation via the splenic nerve restrains the release of inflammatory cytokines from splenic macrophages and helps preserve systemic homeostasis, constituting the efferent cholinergic anti-inflammatory arm of the inflammatory reflex. Our analysis of Danish National Patient Registry data revealed that vagotomy for peptic ulcer disease, particularly truncal vagotomy, markedly increased the risk of developing age-related macular degeneration (AMD). Consistently, experimental truncal vagotomy or splenic denervation in mice exacerbated laser- and light-induced subretinal inflammation, both models of late AMD. The pro-inflammatory effects of vagotomy were abolished by concurrent splenectomy or pharmacologically augmenting acetylcholine signaling. Mechanistically, vagotomy activated a pro-inflammatory transcriptional program in splenic monocytes while suppressing tissue-retention genes *Cxcr4* and *Fn1*, leading to enhanced monocyte egress from the spleen and increased infiltration into the injured retina. In the laser-injured retina, single-cell RNA sequencing (scRNAseq) of mononuclear phagocytes revealed a broad set of vagotomy-induced transcripts in infiltrating monocytes and activated microglia. Remarkably, more than one-third of these were normalized by splenectomy. Together, these findings identify a vagus nerve–spleen–retina axis that connects stress and vagal tone to AMD pathogenesis.

Keywords (10 max)

age-related macular degeneration, neuroinflammation, monocytes, microglia, vagus nerve, vagal tone, inflammatory reflex, cohort study

Graphical abstract

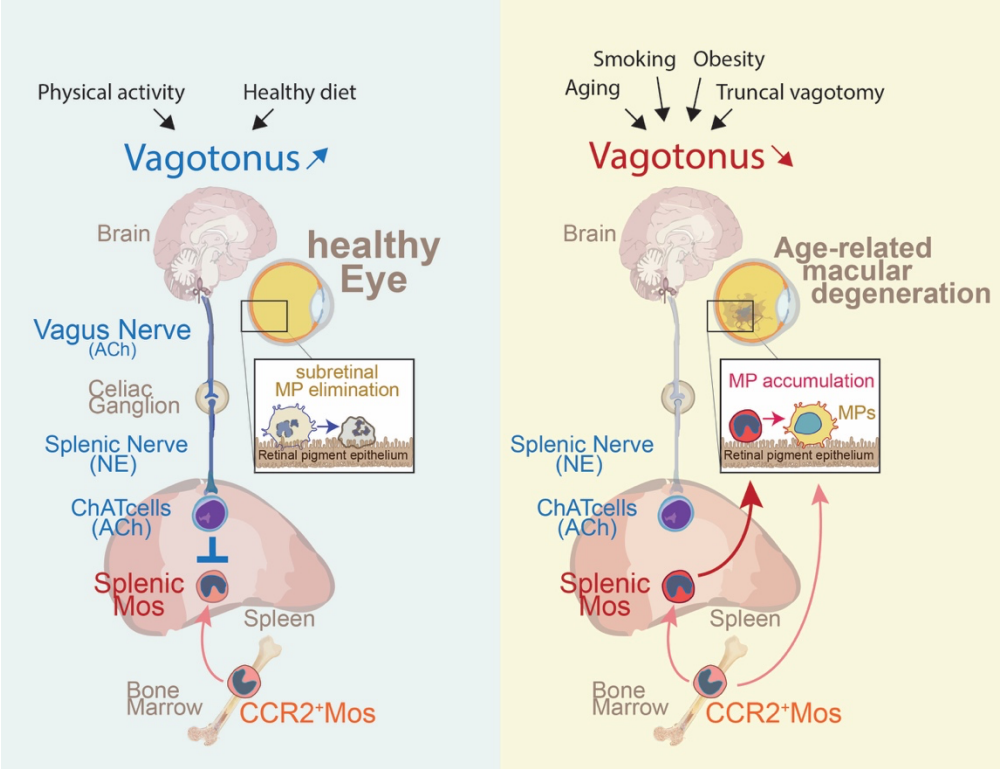

In Brief

Using population-level human data and complementary mouse models, this study demonstrates that loss of vagal signaling enhances subretinal inflammation and increases susceptibility to age-related macular degeneration (AMD). Mechanistically, vagotomy reprograms splenic monocytes toward a pro-inflammatory state, promoting their egress and infiltration into the injured retina, where they amplify local inflammation. These effects identify a vagus nerve–spleen–retina axis that links reduced vagal tone to AMD pathogenesis.

Highlights

- Vagotomy increases AMD risk in humans and exacerbates subretinal inflammation in mouse models of late-stage AMD.
- Loss of vagal signaling drives pro-inflammatory reprogramming and enhanced egress of splenic monocytes via suppression of tissue-retention genes.
- Single-cell transcriptomics reveals vagotomy-induced inflammatory signatures in retinal monocytes and microglia that are largely reversed by splenectomy.

Background

Age-related macular degeneration (AMD) arises from age, genetic, and environmental factors. Early disease is marked by subretinal deposits (pseudodrusen and soft drusen), and progression leads to debilitating choroidal neovascularization (CNV, neoAMD) or an extending area of outer retinal degeneration (geographic atrophy, GA) (Guillonneau et al., 2017). VEGF inhibition suppresses CNV, but complement factor 3 or 5 blockade provides little benefit for neurodegeneration in GA, and all require burdensome lifelong repeated injections.

A shared pathogenic axis across AMD forms is chronic inflammation (Guillonneau et al., 2017; Yu et al., 2020). In AMD, microglia (MC) become activated and, along with monocyte-derived macrophages (MdMs), infiltrate the photoreceptor layer that is normally devoid of immune cells (Guillonneau et al., 2017; Lad et al., 2015; Sennlaub et al., 2013). The three major genetic risk factors, APOE2 (Levy et al., 2015), a CFH variant (Calippe et al., 2017), and 10q26-driven HTRA1 overexpression in MPs (Beguier et al., 2020), promote this MP accumulation (Beguier et al., 2020; Calippe et al., 2017; Levy et al., 2015). In early disease MPs may contribute to debris clearance, but in advanced AMD age-related, genetic, and environmental factors promote their pathogenic polarization. In animal models, infiltrating activated MPs release inflammatory cytokines and reactive oxygen species that drive CNV, accelerate photoreceptor loss, and amplify inflammation by recruiting additional MPs (Guillonneau et al., 2017). MdMs in general and particularly those derived from splenic monocytes, are especially pathogenic in these models (Roubeix et al., 2024; Sennlaub et al., 2013).

Evidence from human studies supports similar mechanisms. Circulating monocytes from patients with AMD display elevated CCL2, IL-8, VEGFA, and IL-6 expression, among other transcriptional alterations (Grunin et al., 2016; Lechner et al., 2017). Serum IL-6 levels further correlate with AMD incidence and progression (Guillonneau et al., 2017; Nahavandipour et al., 2020) and aqueous humor IL-6 levels are increased in GA (Huang et al., 2025). Consistent with a pathogenic role of mononuclear phagocyte cytokines, Janus kinase (JAK) inhibitors, which block IL-6, GM-CSF, IFN-γ, and other pro-inflammatory cytokines signaling, are associated with reduced AMD incidence (Hallak et al., 2024). Collectively, these findings highlight both local and systemic inflammation as central drivers of AMD pathogenesis.

One important regulator of the immune system is the inflammatory reflex, a vagus nerve–mediated neuroimmune pathway that senses peripheral inflammation and suppresses excessive

95 cytokine production, thereby maintaining immune homeostasis. In its cholinergic anti-
96 inflammatory efferent arm, parasympathetic signals from the vagus nerve stimulate the splenic
97 nerve at the coeliac ganglion, increasing norepinephrine release in the spleen. This stimulates
98 acetylcholine release from choline acetyltransferase (ChAT)-expressing T cells, which activates
99 α7 nicotinic acetylcholine receptors on splenic macrophages, delivering a tonic inhibitory signal
100 that suppresses macrophage activity and limits the release of proinflammatory cytokines into the
101 circulation (Andersson & Tracey, 2012; Chavan et al., 2017). Disruption of this reflex by truncal
102 vagotomy in animals leads to disproportionate cytokine responses and increased mortality during
103 sterile endotoxic shock, whereas vagal nerve stimulation improves survival (Borovikova et al.,
104 2000). In humans, truncal vagotomy has been linked to an increased incidence of RA (Baker et al.,
105 2025), whereas implantable vagus nerve stimulation has been shown to reduce disease severity
106 and was recently granted FDA premarket approval (PMA number P240039) (Koopman et al.,
107 2016). It remains unclear, however, whether the protective effect of high vagal tone in RA is
108 mediated through regulation of systemic cytokine release or through other, as yet unidentified,
109 anti-inflammatory mechanisms.

110 Vagal tone diminishes with aging, smoking and obesity (Andersson & Tracey, 2012; Bodin
111 et al., 2017), the main non-genetic AMD risk factors (Fleckenstein et al., 2021), and increases with
112 aerobic exercise, which protects against AMD (Andersson & Tracey, 2012; McGuinness et al.,
113 2017). We recently demonstrated that reduced heart rate variability, reflecting impaired vagal tone,
114 is associated with neoAMD (Molbech et al., 2025). This observation suggests that individuals with
115 AMD may exhibit diminished vagal activity, which could contribute to a dysregulated
116 inflammatory reflex, heightened inflammatory responses, and progression of the disease.

117 Here we demonstrate that truncal vagotomy is associated with an increased risk of AMD
118 in humans, and that experimental vagotomy or splenic denervation in mice exacerbated subretinal
119 inflammation. These pro-inflammatory effects depended on an intact cholinergic anti-
120 inflammatory pathway and were abolished by splenectomy or by inhibition of acetylcholine
121 degradation. Mechanistically, vagotomy reprogrammed splenic monocytes and promoted their
122 mobilization, leading to exacerbated retinal inflammation, Together, these findings define a
123 vagus–spleen–retina axis that links vagal tone to splenic monocyte mobilization and pathogenic
124 macrophage infiltration in AMD pathogenesis, and highlight potential therapeutic targets.

Results

Vagotomy is associated with increased incidence of AMD

To investigate whether loss of vagal tone influences the risk of age-related macular degeneration (AMD), we performed a nationwide cohort study using Danish National Patient Registry data (Fig. 1A). Although advances in medical therapy, including antibiotics and proton pump inhibitors, have largely rendered vagotomy obsolete, the procedure was commonly performed for peptic ulcer disease in Denmark between 1977 and 1995 (Lagoo et al., 2014; Svensson et al., 2015). Two vagotomy procedures were analyzed: truncal vagotomy (TV), which involves cutting the vagus nerves inferior to the esophageal hiatus and denervates major abdominal organs including the spleen, and superselective vagotomy (SSV), which cuts only gastric branches while largely sparing innervation of other abdominal organs, including the spleen (Fig. 1A). These procedures provided two patient groups with similar indications for surgery but differing degrees of systemic vagal denervation.

The study cohort included 9,465 patients who underwent vagotomy with at least 10 years of follow-up: 4,040 underwent TV, 5,080 underwent SSV, and 345 had unspecified vagotomy (Supplemental Table 1). A comparison cohort of 85,930 age- and sex-matched individuals from the general population was randomly sampled at a 10:1 ratio for each vagotomized patient. The index date for the comparison cohort was defined as the date of vagotomy in the matched patient. Patients with AMD diagnosed prior to the index date were excluded from all analyses.

During follow-up, vagotomy was associated with a higher cumulative incidence of AMD. After adjustment for age, sex, chronic obstructive pulmonary disease (COPD, as a proxy for smoking), hypertension, obesity-related diseases, and 19 Charlson Comorbidity Index (CCI) categories, the overall adjusted hazard ratio (aHR) for AMD was 1.36 (Table 1, Figure 1B, Supplemental Table 2). When examining TV and SSV separately, SSV was associated with only a modest increase in AMD incidence (2.47 per 1,000 person-years vs. 2.09 in its comparison cohort), whereas TV was associated with a substantially higher incidence (3.85 per 1,000 person-years vs. 2.85 in its comparison cohort) and an aHR of 1.45 (Table 1, Figure 1C-D, Supplemental Table 2).

The lack of a pronounced association in the SSV cohort suggests that the increased risk of AMD observed in TV patients is unlikely to be driven solely by peptic ulcer disease or by vagotomy-induced changes in gastric acidity, or other important peptic ulcer risk factors such as

156 smoking, which are common to both procedures. Instead, the data indicate that broader abdominal
157 denervation, including the splenic branch of the vagus nerve, may underlie the observed increase
158 in AMD incidence.

159 Vagotomy promotes inflammation and exacerbates disease severity in mouse models of
160 AMD in a spleen-dependent manner

161 Our data identified truncal vagotomy as an AMD risk factor, implicating reduced vagal
162 tone in disease pathogenesis, in agreement with evidence that the AMD-risk factors age, smoking,
163 and obesity depress vagotonus, whereas aerobic exercise protects against AMD and increases
164 vagotonus (Andersson & Tracey, 2012; Bodin et al., 2017; Fleckenstein et al., 2021; McGuinness
165 et al., 2017). Physiologically, parasympathetic vagal output activates the adrenergic splenic nerve
166 at the celiac ganglion, triggering acetylcholine release from ChAT^{+} T cells. This provides a tonic
167 inhibitory signal that suppresses proinflammatory cytokine production by splenic macrophages
168 and may exert additional spleen-dependent anti-inflammatory effects (Andersson & Tracey, 2012;
169 Chavan et al., 2017) (Fig. 2A). To model reduced vagal tone, we used left cervical truncal
170 vagotomy, which strongly reduces splenic nerve activity in mice (Carnevale et al., 2016).

171 In humanized transgenic mice expressing the AMD-risk APOE2 isoform (TRE2 mice),
172 vagotomy at 3 months of age increased age-associated subretinal IBA1^{+} MP accumulation that
173 characterizes this model (Calippe et al., 2017; Levy et al., 2015) measured at 13 months on
174 RPE/choroidal flatmounts (Fig. 2B). In the laser-induced subretinal inflammation and choroidal
175 neovascularization model (the standard model of neoAMD) in 3–month-old male C57BL/6J mice,
176 vagotomy (performed one month before laser to allow for complete recovery) increased IBA1^{+}
177 MP accumulation and CD102^{+} CNV area quantified on RPE/choroidal flatmounts. Concomitant
178 splenectomy normalized both parameters to levels observed in sham-operated controls,
179 demonstrating a spleen-dependent effect (Fig. 2C).

180 We next performed a series of experiments to determine if the pro-inflammatory effect of
181 vagotomy was mediated via the inflammatory reflex. First, denervating the spleen by ethanol
182 application at the splenic hiatus in 2-month-old male C57BL/6J mice (one month before laser to
183 allow for recovery), confirmed by loss of tyrosine-hydroxylase (TH) staining on spleen sections
184 (Fig. 2D, left), increased laser-induced IBA1^{+} MP accumulation and CD102^{+} CNV on
185 RPE/choroidal flatmounts relative to sham, phenocopying vagotomy and confirming splenic nerve
186 involvement (Fig. 2E, right). Second, vagotomy failed to augment subretinal MPs or CNV after

187 laser in 3-month-old male *Rag2*$^{-/-}$ mice, which lack mature lymphocytes including ChAT^{+} T cells
188 but continue to harbor pathogenic splenic monocytes (Roubeix et al., 2024) (Fig. 2E).
189 Next, mice received daily intraperitoneal injections of the acetylcholinesterase inhibitor
190 galantamine after laser to restore acetylcholine availability diminished by vagotomy and reduced
191 ChAT-cell output. This reversed the pro-inflammatory phenotype, returning subretinal MP counts
192 and CNV size to sham in the laser CNV model, similar to splenectomy (Fig. 2F). Further, 3-month-
193 old male TRE2 mice were exposed to a calibrated bright-light challenge, which induces MP
194 infiltration in TRE2 mice but not in controls and within a shorter time frame than in the
195 experiments shown in Fig. 2B (Calippe et al., 2017; Levy et al., 2015). Quantification of IBA1+
196 MPs on RPE flatmounts revealed that vagotomy also increased MP accumulation in this model,
197 an effect again abrogated by splenectomy and reversed by galantamine (Fig. 2G).
198 Collectively, our results demonstrate that disrupting vagus-to-spleen cholinergic signaling
199 through truncal vagotomy amplifies subretinal MP responses and CNV. This effect requires both
200 splenic innervation and lymphocytes, most likely ChAT^{+} T cells, and it can be reversed by
201 enhancing acetylcholine tone, consistent with the cholinergic efferent arm of the inflammatory
202 reflex. Notably, these findings in animal models parallel the finding in the cohort study that truncal
203 vagotomy promoted AMD pathogenesis (Fig.1).
204 Loss of vagal tone reshapes the splenic monocyte transcriptome and drives their
205 mobilization
206 The spleen functions as a major reservoir of CCR2^{+}Ly6C^{high} monocytes (SpleMos)
207 (Swirski et al., 2009), which, together with circulating Ly6C^{high} monocytes, are recruited into
208 diseased tissues (Robbins et al., 2012; Swirski et al., 2009) where they differentiate into
209 inflammatory MdMs. We recently demonstrated that SpleMos play a particularly pathogenic role
210 in retinal inflammation in AMD (Roubeix et al., 2024), analogous to their established role in
211 atherosclerosis (Robbins et al., 2012). On this basis, we next examined cellular and molecular
212 changes in the spleen, focusing specifically on potentially pathogenic splenic monocytes following
213 the loss of vagal tone.
214 Flow cytometric analysis of spleens from 3-month-old mice, performed 30 days after
215 vagotomy, revealed no differences in the numbers of CD45^{+}CD11b^{+} MPs, CD45^{+}CD11b^{+}Ly6C^{high}
216 monocytes (Mos), or CD4^{+} and CD8^{+} T cells compared with sham-operated controls (Fig. 3A,
217 Supplemental Fig. 1). Bulk RNA sequencing of FACS-sorted CD45^{+}CD11b^{+}Ly6C^{high}Ly6G^{neg}

218 splenic Mos identified 508 upregulated and 1860 downregulated genes in splenic Mos from
219 vagotomized mice compared with sham-operated controls (Fig. 3B, Supplemental Table 5).
220 Classical monocyte markers, including *Ccr2*, *Ly6c2*, *Cd14*, and *Sell*, were expressed at comparable
221 levels between groups (Fig. 3C). In contrast, several genes associated with immune defense were
222 upregulated in Mos from vagotomized mice, such as MHC class II-related genes (*H2-Aa*, *CD74*)
223 and pattern recognition receptors (*Clec4g*, *CD209e*) (Fig. 3D). Several pro-inflammatory genes
224 were also upregulated, including *Il1b*, *Lilra5*, *Ccl4*, and *C5ar1* (Fig. 3E). Conversely, among the
225 1860 downregulated genes were several implicated in monocyte retention. These included two of
226 the most strongly regulated genes, *Fn1*, whose autocrine expression anchors endothelial cells
227 within the extracellular matrix (Cseh et al., 2010), and *Cxcr4*, a central mediator of bone marrow
228 monocyte retention (Chong et al., 2016), along with the integrins *Itga4* and *Itga1* (Fig. 3F).
229 To assess how vagal denervation affects monocyte efflux from the spleen, we analyzed
230 spleens of vagotomized mice with or without laser injury at day 1 (Fig. 3G). In the spleen, prior to
231 laser injury, the number of Ly6C^{high} monocytes did not differ between groups, as quantified by
232 flow cytometry. However, one day after laser treatment, spleens from vagotomized mice showed
233 a marked reduction in monocyte numbers, indicating enhanced efflux in response to injury (Fig.
234 3G).
235 Together, these findings suggest that disruption of vagal signaling alters the splenic
236 monocyte transcriptome toward enhanced immune defense and a pro-inflammatory profile,
237 potentially influencing their polarization upon infiltration into diseased tissues. Importantly,
238 vagotomy increased the mobilization of splenic Mos before the vagotomy-induced, spleen-
239 dependent increase in subretinal inflammation that we observed (Fig. 2).
240 Vagotomy induces transcriptional reprogramming of infiltrating monocytes and activated
241 microglia in the retina in a spleen-dependent manner
242 Since vagotomy altered the splenic monocyte transcriptome, enhanced their mobilization
243 (Fig. 3), and promoted spleen-dependent accumulation of chorio-retinal MPs (Fig. 2), we next
244 investigated how vagotomy-primed splenic monocytes influence the composition and polarization
245 of resident and infiltrating MPs during sterile chorio-retinal inflammation. We performed single-
246 cell RNA sequencing on sorted CD45^{+}CD11b^{+} cells from posterior eye cups from vagotomized or
247 sham operated mice one day after laser injury or without laser-injury (Fig. 4A). Using Seurat for
248 dimensionality reduction with principal component analysis (PCA), UMAP, and graph-based

249 clustering, we identified 11 transcriptionally distinct clusters of MPs based on canonical marker
250 gene expression (Fig. 4B). Under homeostatic non-laser conditions (Fig. 4C, upper panel), these
251 clusters were annotated as resident macrophages (*C1qa*^{high}, *Cd68*^{high}) of the choroid (*F13a1*^{high}) or
252 as microglial cells (MCs, *P2ry12*^{high}), as well as circulating monocytes (*Nr4a1*$^{+}$, *Spn*$^{+}$, *Ace*$^{+}$) that
253 segregated into two subsets: patrolling Mos (*Ly6c2*^{low}, *Ccr2*^{low}) and inflammatory Mos (*Ly6c2*^{high},
254 *Ccr2*^{high}). In post-lasered eyes, we additionally observed several subsets of activated MCs,
255 characterized by reduced expression of homeostatic MC genes and upregulation of inflammatory
256 cytokines (*Ccl12*, *Ccl2*) (clusters 2-5, Fig. 4C lower panel). We also detected a large population
257 of infiltrating Mos (cluster 9, *Lgals3*^{high}, *Il1b*^{high}, *Spn*^{low}, *Ace*^{low}), as well as early monocyte-derived
258 macrophages distinguished by increased *Itgax* (Cd11c, cluster 10 and 11) expression. It is
259 important to note that the Seurat-defined clusters are based on a broad transcriptional profile, and
260 these genes are shown here only as representative examples.

261 In non-lasered eyes, vagotomy did not alter the overall cell type composition compared to
262 sham-operated controls. The majority of MPs were homeostatic microglia, accompanied by a small
263 cluster of choroidal macrophages and predominantly patrolling monocytes (Fig. 4D). The
264 activation state of homeostatic microglia also remained unchanged, as evidenced by stable
265 expression of homeostatic markers, absence of activation marker expression, and only limited
266 transcriptional changes, with 20 genes upregulated and 24 genes downregulated between
267 vagotomy and sham conditions (Fig. 4E, Supplemental Table 6).

268 In sharp contrast, the lasered samples were dominated by activated microglia (clusters 2-
269 5) and infiltrating monocytes (clusters 9 and 10; Fig. 4C–D). Within the activated microglial
270 population, several subclusters were detected, but cluster #3 (activated MC 2) was markedly
271 expanded in the vagotomized condition compared to both sham and splenectomy controls,
272 prompting us to focus on this subset (Fig. 4F and G). Relative to sham/sham-operated laser-injured
273 animals, vagotomized/sham laser-injured mice displayed 162 upregulated and 95 downregulated
274 genes in the MC cluster 3 (Fig. 4F). Vagotomized/sham laser-injured mice displayed 74
275 upregulated and 24 downregulated genes relative to VGX/SpleX -operated laser-injured animals
276 (Supplemental Table 7). Strikingly, the vagotomy-induced deregulation of a large proportion of
277 genes (65/162 and 15/95, respectively) was reversed by splenectomy (Fig. 4F, Supplemental Table
278 8). The most regulated genes included *Il6ra*, *B2m*, *Srgn*, *Tlr7*, *C1qb*, and *H2-D1*, covering
279 pathways in cytokine signaling, antigen presentation, proteoglycan-mediated granule biology,

280 innate immune sensing, complement activation, transcriptional regulation, and MHC class II
281 presentation. Similarly, in infiltrating monocytes, we identified 330 upregulated and 82
282 downregulated genes in vagotomized/sham laser-injured mice, of which 105 and 21, respectively,
283 were normalized in VGX/SpleX laser-injured animals (Fig. 4G, Supplemental Tables 9-10). The
284 most regulated genes included *Jak2*, *Id2*, *Srgn*, *Vcan*, *Clec4d*, and *Filip1l*, which are associated
285 with cytokine signaling, transcriptional control, granule biology, extracellular matrix organization,
286 pathogen recognition, cytoskeletal regulation, and immune modulation.

287 Taken together, vagotomy had minimal impact on the transcriptome of MPs in uninjured
288 eyes. By contrast, following laser injury, which recruits, in part, spleen-derived monocytes
289 (Roubeix et al., 2024), vagotomy induced transcriptional changes in infiltrating monocytes but
290 also activated microglia. Notably, splenectomy reversed a substantial fraction of these
291 transcriptional changes.

Discussion

Factors known to reduce vagal tone, such as aging, smoking, and obesity (Andersson & Tracey, 2012; Bodin et al., 2017), are also established risk factors for AMD (Fleckenstein et al., 2021). In line with this, we recently reported that reduced heart rate variability, a marker of vagal tone, is associated with AMD (Molbech et al., 2025). In the present study, we demonstrated that the surgical vagotomy, once used in the treatment of peptic ulcers, is associated with an increased risk of AMD (all forms combined), independently of age, smoking, and obesity (Fig.1). Superselective vagotomy was associated with only a modest risk increase compared to the substantial risk increase of truncal vagotomy, supporting the interpretation that the observed association with truncal vagotomy is not attributable to peptic ulcer disease or related risk factors such as smoking, which are similarly distributed between the two patient groups.

Since truncal, but not superselective, vagotomy profoundly reduces vagal tone in the spleen, and truncal vagotomy (but not superselective) has recently been linked to the incidence of autoimmune rheumatoid arthritis (Baker et al., 2025), we hypothesized that the observed association of truncal vagotomy with AMD risk is driven by disruption of the anti-inflammatory effect of the vagus nerve on the spleen. Indeed, experimental cervical truncal vagotomy in mice, which markedly reduces splenic nerve activity (Carnevale et al., 2016), led to increased subretinal inflammation following laser injury, as well as exaggerated age-related MP accumulation observed in TRE2 mice expressing the AMD risk gene *APOE2* (Levy et al., 2015) (Fig. 2B-C). Importantly, splenectomy reversed the vagotomy-induced exaggerated inflammation in laser-induced subretinal inflammation and in light induced inflammation in *APOE2*-expressing mice (Fig. 2F-G), highlighting the spleen's pivotal role in mediating the proinflammatory effects of vagotomy.

We performed a series of experiments to examine if the pro-inflammatory effect of vagotomy is propagated via the disturbance of the inflammatory reflex (Fig. 2A). Splenic denervation alone was sufficient to amplify the laser-induced inflammatory response (Fig. 2D), suggesting that in our model parasympathetic anti-inflammatory influence outweighs the sympathetic tone transmitted through the splenic nerve, consistent with observations of splenic denervation in the endotoxin shock model (Rosas-Ballina et al., 2008). Acetylcholinesterase inhibitor galantamine administration, to restore acetylcholine levels decreased by both diminished vagotonus in the celiac ganglion and from $ChAT^+$ T cells in the spleen, also reversed the effect of vagotomy in both models (Fig 2F-G). Interestingly, use of anticholinergic drugs has previously

323 been associated with AMD (Aldebert et al., 2018), which our findings suggests might be mediated
324 at least in part by a loss of cholinergic signaling in the anti-inflammatory reflex.
325 The finding that vagotomy failed to augment laser-induced subretinal MPs or CNV in
326 *Rag2*$^{-/-}$ mice, which lack mature lymphocytes (Shinkai et al., 1992) including ChAT^{+} T cells but
327 still maintain splenic monocytes (Roubeix et al., 2024), further supports ChAT^{+} T-cell dependence
328 (Fig. 2E). However, in contrast to severe sterile endotoxic shock (Borovikova et al., 2000), we did
329 not observe vagotomy-induced excessive cytokine release by splenic macrophages (data not
330 shown) likely because localized ocular laser injury was not sufficient to increase cytokine release
331 from splenic macrophages contrary to endotoxic shock. Taken together this set of experiments
332 demonstrates that experimental vagotomy in mice aggravates AMD models and confirms the
333 clinical observation of truncal vagotomy association with AMD. Further, it establishes a pivotal
334 role of the spleen in mediating this effect.
335 In the spleen, under homeostatic conditions and in the absence of laser injury, vagotomy
336 did not alter the numbers of MPs, T cells, or monocytes (Fig. 3A, Supplemental Fig. 1). Given that
337 CD45^{+}CD11b^{+}Ly6C^{high} splenic monocytes play a particularly pathogenic role in retinal
338 inflammation in AMD (Roubeix et al., 2024), we next analyzed their transcriptome. Several pro-
339 inflammatory genes (*Il1b*, *Lilra5*, *Ccl4*, and *C5ar1*), as well as genes linked to immune defense
340 (MHC class II genes and pattern recognition receptors), were upregulated in splenic monocytes
341 after vagotomy compared to sham-operated animals (Fig. 3B-E). These findings raise the
342 possibility that vagal innervation provides a tonic inhibitory input to splenic monocytes, potentially
343 mediated by currently unidentified signals from splenic macrophages, beyond its previously
344 established effects on macrophage cytokine release (Andersson & Tracey, 2012; Chavan et al.,
345 2017). Notably, the most strongly regulated genes included downregulation of *Cxcr4*, a central
346 mediator of bone marrow monocyte retention (Chong et al., 2016) and Fibronectin 1 (*Fn1*), whose
347 autocrine expression anchors endothelial cells within the extracellular matrix (Cseh et al., 2010),
348 along with fibronectin-binding *Itga4* and collagen-binding *Itga1* (Fig. 3F). Given that the spleen
349 serves as a major reservoir for Ly6C^{high} monocytes (SpleMos) (Swirski et al., 2009), we next tested
350 whether these transcriptional changes translated into altered monocyte egress during
351 inflammation. Flow cytometric analysis revealed a marked reduction in splenic Ly6C^{high}
352 monocytes in vagotomized mice compared with sham-operated controls one day after laser injury,
353 consistent with enhanced egress (Fig. 3G).

354 Because vagotomy reprograms splenic monocytes, increases their mobilization (Fig. 3),
355 and amplifies spleen-dependent subretinal MP accumulation (Fig. 2), we next examined how these
356 primed cells influence MP composition and polarization during sterile chorio-retinal
357 inflammation. In eyes without laser injury, vagotomy produced only minimal transcriptional
358 alterations in the homeostatic microglia and choroidal macrophages (Fig. 4B-E). In contrast, laser-
359 induced injury led to the infiltration of monocytes and the appearance of several activated
360 microglial subtypes (Fig. 4B-D). Notably, vagotomy selectively increased the relative abundance
361 of activated MC2 (cluster #3) in a spleen-dependent manner, demonstrating that signals derived
362 from the spleen are required for this effect. A plausible possibility is that infiltrating spleMos
363 convey these signals; however, directly and specifically labeling spleMos remains technically
364 challenging. Subcapsular red pulp dye injections, similarly to intravenous injections, also label
365 classical circulating blood monocytes. Likewise, spleMos from transplanted GFP^{+} spleens are
366 replaced by GFP^{-} recipient spleMos before the host has fully recovered from surgery. Finally,
367 photoconversion of subcapsular spleMos in *Cx3cr1*^{Dendra2} mice (Miller et al., 2021) proved either
368 inefficient or excessively damaging at the ultraviolet intensities required in our hands. Technical
369 advancements and further studies will be necessary to decipher the specific molecular and
370 signaling pathways by which spleMos or other signals from the spleen modulate microglial
371 activation after vagotomy.
372 In both infiltrating monocytes and activated MCs, the differentially expressed genes
373 regulated by vagotomy were predominantly upregulated. Strikingly one-third of these changes
374 reverted to baseline after splenectomy, underscoring the necessity of the efferent arm of the
375 inflammatory reflex and the spleen.
376 Together, our demonstration of the involvement of the inflammatory reflex in AMD
377 pathogenesis points to several novel therapeutic strategies. In addition to pharmacological
378 inhibition of acetylcholinesterase the avoidance of anticholinergic drugs, our findings suggest that
379 AMD patients may benefit from therapeutic vagus nerve stimulation, which has been shown to
380 reduce neuroinflammation and modulate microglial polarization in rodent models of spinal cord
381 injury (Chen et al., 2022) and stroke (Zhang et al., 2021).

382 ## Conclusions

383 In conclusion, we demonstrate that vagotomy is associated with an increased
384 incidence of AMD in a human patient cohort and exacerbates pathogenic inflammation in mouse

385 models of the disease. Mechanistically, this effect stems from an exaggerated, spleen-dependent
386 inflammatory response that profoundly alters the chorioretinal mononuclear phagocyte response
387 during retinal inflammation. The pro-inflammatory consequences of experimental vagotomy can
388 be mitigated by splenectomy and pharmacological enhancement of parasympathetic signaling.
389 Together, these findings provide mechanistic insight into how systemic factors such as aging and
390 obesity may increase the risk of AMD, and they confirm cholinergic drugs and vagus nerve
391 stimulation as potential therapeutic strategies to dampen excessive inflammation in AMD and
392 other conditions associated with dysregulation of the inflammatory reflex.

Methods

Danish National Patient Registry cohort study

We conducted a population-based nationwide cohort study using Danish administrative registry data, following principles similar to those in previous epidemiological studies (Svensson et al., 2015). Denmark's tax-funded healthcare system provides all residents with free, unlimited access to diagnostic work-up and treatment, including for AMD. The Civil Registration System (CRS) assigns all residents a unique identification number, enabling linkage across national registries (Schmidt et al., 2014; Schmidt et al., 2019).

All patients undergoing vagotomy (TV or SSV) between January 1, 1977 and December 31, 1995 were identified via procedural codes in the Danish National Patient Registry (DNPR; Supplemental Table 4). AMD cases were identified with ICD-8 and ICD-10 codes (Supplemental Table 3). Although surgical procedures are generally coded with high accuracy, no validation studies have specifically assessed the accuracy of DNPR procedure codes for vagotomy, so although unlikely misclassification is therefore possible. However, the most likely misclassification, if any, would be the coding of a vagotomy despite incomplete resection. Thus, misclassification, if any, is expected to bias estimated associations towards the null (Svensson et al., 2015).

For each vagotomized patient, up to ten age- and sex-matched individuals from the general population who had not undergone vagotomy were randomly sampled. The index date for each control was defined as the date of vagotomy in the matched patient. Persons in the comparison cohort who underwent vagotomy after the index date were reclassified into the vagotomy cohort. Individuals with pre-existing AMD were not included in the cohorts.

Comorbidities were assessed via linkage to Danish National Patient Registry data according to 19 major disease categories from the Charlson Comorbidity Index (CCI; Supplemental Table 3). Peptic ulcer disease was excluded from the CCI because it was present in nearly all vagotomized patients. Comorbidity burden was classified as normal (0), moderate (1–2), or severe (3+), according to the number of comorbid categories present.

All participants were followed from the index date until AMD diagnosis, death, emigration, or December 31, 2012, whichever occurred first. Cumulative incidence curves were generated using Kaplan-Meier analysis with death treated as a competing risk and smoothed for visualization using splines. Because proportional hazards assumptions were not met in the first five years,

424 analyses were restricted to patients surviving ≥10 years after vagotomy and their matched controls.
425 Hazard ratios for AMD were estimated with Cox proportional hazards regression, adjusted for age,
426 sex, COPD, hypertension, obesity-related diseases, and CCI category. Sensitivity analyses were
427 performed, stratified by COPD as a proxy for smoking, by obesity-related diseases, and by
428 hypertension. E-values were calculated to assess the potential effects of unmeasured confounders,
429 such as smoking (VanderWeele & Ding, 2017).

430 The study is registered at Aarhus University's Record of Processing Activities (j.nr. 2022-
431 0367531, record number 2234). Studies based exclusively on data from the Danish national
432 registers do, by Danish legislation, not require approval from the Danish Health Research Ethics
433 committees.

434 Animals

435 C57BL/6J mice (Jax strain #000664) were purchased from the Janvier Breeding Center.
436 *TRE2* mice, which express the human APOE2 isoform, were engineered using targeted
437 replacement as previously described (Levy et al., 2015). *Rag2*$^{-/-}$ mice were purchased from Charles
438 River Laboratories (Jax strain #008449). All mice were negative for the *Crb1*^{rd8}, *Pde6b*^{rd1}, and
439 *Gnat2*^{cpfl3} mutations. Mice were housed under specific pathogen-free conditions in a 12 hr/12 hr
440 light/dark cycle with water and food available ad libitum. All experimental protocols and
441 procedures were approved by the French Ministry of Higher Education, Research and Innovation
442 (APAFIS authorization #19412 2019022215422220).

443 Surgeries (vagotomy, splenectomy, splenic denervation, and sham)

444 Mice received a subcutaneous injection of buprenorphine (0.05 mg/kg) 30 minutes before
445 surgery, then were anesthetized with a mixture of ketamine (80 mg/kg) and xylazine (8 mg/kg).
446 Mice received a second subcutaneous injection of buprenorphine (0.05 mg/kg) the day after
447 surgery. Antiseptic solution (Vetedine, povidone iodine) was applied to all skin sutures
448 immediately after closure. Mice were allowed to fully recover for at least 1 month following
449 surgery before any further experiments.

450 For vagotomies, a 1 cm midline cervical incision was made, the left vagus nerve was cut,
451 and then the incision was closed with absorbable sutures. For sham vagotomies the left vagus nerve
452 was visualized but not cut, and were otherwise identical.

453 Splenectomies and sham splenectomies were performed as previously described (Roubeix
454 et al., 2024). In brief, a 1 cm incision was made on the left side of the abdomen under the rib cage,

455 the spleen was removed by cutting the connective tissue and cauterizing the splenic vessels (or
456 only visualized without removal for sham splenectomies), and finally the incisions in the
457 abdominal muscles and skin were each closed with absorbable sutures.

458 Splenic denervation was achieved using ethanol, similarly to previous studies (Zhang et
459 al., 2020). In brief, an incision was made in the left abdomen as for splenectomy, and then the
460 spleen was isolated from the abdominal cavity using blunt forceps, while cotton pads moistened
461 with physiological saline were used to protect the abdominal opening and organs. Splenic
462 denervation was achieved by applying a cotton swab dipped in absolute ethanol to the vascular
463 trees and corresponding nerve fibers, approximately 7 times, 5-10 seconds per application. For
464 sham denervation the cotton swab was instead dipped in physiological saline solution (0.9% NaCl).
465 Finally, the spleen was returned to the abdominal cavity and incisions were closed as for
466 splenectomies.

467 Laser injury and bright light challenge

468 Laser injury and bright light challenge were performed as previously described (Roubeix
469 et al., 2024). For laser injury, mice received eye drops of mydriaticum and neosynephrine to dilate
470 the pupils, and then were anesthetized with a mixture of ketamine (80 mg/kg) and xylazine (8
471 mg/kg). Lubrithal was placed on the eye to maintain ocular surface moisture. For
472 immunohistochemistry 4 laser injuries were performed per eye in the mid-periphery using a
473 photocoagulation laser (Vitra Laser, 532 nm, 450 mW, 50 ms, 250 mm). For single-cell RNA
474 sequencing and flow cytometry experiments, 10 laser injuries were performed per eye. For bright
475 light challenge, the *TRE2* mice received daily eyedrops of atropine (1%, Novartis) to dilate their
476 pupils, and were exposed to green LED light (4500 lux) for 4 days.

477 Immunohistochemistry

478 Eyes were fixed in 4% PFA at room temperature (RT) for 45 minutes before storage in
479 PBS and dissection. Anterior segments and lens were removed, and after 4 curvature-relieving cuts
480 were made the retinas and RPE/choroid/sclera were carefully separated and then incubated
481 overnight at RT in PBS with 1% Triton X-100 with the following primary antibodies (dilutions
482 indicated in parentheses): rabbit anti-IBA1 (Wako, 1:400) and rat anti-CD102 (BD Biosciences,
483 1:200). After 3 PBS rinses, retinas and RPE/choroid/sclera complexes were incubated for 2 hours
484 at RT with Alexa Fluor-conjugated secondary antibodies (Thermo Fisher Scientific, diluted 1:500)
485 and Hoechst (Sigma Aldrich, diluted 1:1000) in PBS. After 3 more PBS rinses, tissues were

486 flatmounted and coverslipped with an aqueous mounting medium (Sigma Aldrich) and imaged
487 using a fluorescence microscope (Leica, DM5500). Quantifications of MP counts and CNV size
488 were completed in FIJI. MPs and CNV size were quantified for individual laser impacts and were
489 then averaged by eye for further statistical analyses and graphical representation.

490 For spleen cryosections, spleens were flash frozen in liquid nitrogen, embedded in Neg-50
491 optimal cutting temperature compound (Fischer Scientific), and then 12 µm sections were cut on
492 a Leica CM3050 cryostat. Sections were fixed on the slide with 4% PFA for 15 minutes at RT,
493 blocked for 1 hour at RT in blocking solution (PBS + 0.1% Triton X-100 + 5% normal horse
494 serum), and then incubated overnight at 4 C with rabbit anti-tyrosine hydroxylase (Sigma-Aldrich,
495 1:200) and human anti-mouse CD3 (REAfinity, PE-conjugated, Miltenyi, 1:100) diluted in
496 blocking solution. After 3 PBS rinses, sections were incubated for 2 hours at RT with Alexa Fluor-
497 conjugated secondary antibodies (Thermo Fisher Scientific, 1:500) and Hoechst (Sigma Aldrich,
498 1:1000) in blocking solution. After 3 more PBS rinses slides were coverslipped with an aqueous
499 mounting medium (Sigma Aldrich) and imaged using a fluorescence microscope (Leica,
500 DM5500).

501 Galantamine treatment

502 Galantamine, an acetylcholinesterase inhibitor (Sigma Aldrich), was resuspended in
503 physiological 0.9% NaCl solution at a concentration of 1 mg/ml and then mice were given daily
504 IP injections of Galantamine (4 mg/kg) or an equal volume of saline for control.

505 Flow cytometry and fluorescence-activated cell sorting

506 Flow cytometry of eyes and spleens was performed as previously described (Roubeix et
507 al., 2024). In brief, spleens were mechanically dissociated on a 70-µm cell strainer (Miltenyi), red
508 blood cells were lysed using ammonium chloride (StemCell Technologies), and after rinsing in
509 PBS and centrifugation (500 g, 5 min, 4 C), cells were resuspended in PBS. Eyes were dissected
510 to remove posterior connective tissue from the sclera, the anterior segment, and the lens, and the
511 resulting posterior segment eye cups were enzymatically dissociated using Liberase TL in PBS
512 (0.8 Wunsch unit/ml, Sigma-Aldrich) followed by gentle mechanical dissociation using a P1000
513 pipette. The resulting cell suspension was passed through a 70-µm filter, rinsed with PBS, and
514 resuspended in PBS following centrifugation (500 g, 5 min, 4 C). Cells were labeled using a
515 live/dead fixable reagent (Miltenyi) following manufacturer recommendations, then incubated
516 with the relevant antibodies (all diluted 1/50 in PBS) for 30 minutes at 4 C. The antibodies used in

517 this study include: anti-CD45 VioBlue, anti-CD11b PE, anti-Ly6C PE-Vio770, anti-Ly6G APC-
518 Vio770, anti-CD3 FITC, anti-CD8a PE, and anti-CD4 PE-Vio770 (all from Miltenyi). For flow
519 cytometry, cells were fixed in 1% PFA, data acquisition was performed on a Celesta SORP
520 cytometer (BD Biosciences), and data were analyzed with FlowJo 10.9. For cell sorting, cells
521 suspensions were prepared as described for flow cytometry but without the final fixation step.
522 Cells were sorted into chilled tubes using a FACSMelody cell sorter (BD Biosciences).

523 Bulk mRNA sequencing

524 $CD11b^{+}CD45^{+}Ly6C^{neg}Ly6C^{high}$ splenic monocytes were sorted, as described above. RNA
525 was extracted and RNA quality was confirmed using a Bioanalyzer RNA Analysis kit (Agilent).
526 RNA sequencing libraries were prepared from 2 ng total of RNA using the Smartseq V4 (Takara)
527 and Nextera XT (Illumina) kits and sequenced at the Institut du Cerveau iGenSeq sequencing
528 facility.

529 After sequencing, fastq files were aligned to the *Mus musculus* reference genome from
530 Ensembl (Ensemble 106, June 2022) using STAR (version 2.7.9a) with the option "- - quantMode
531 Gene Counts" to extract the raw counts for each gene, and all count files were concatenated into a
532 single file. The count file and descriptive sample file were loaded into our in-house R Shiny
533 application "EyeDVseq" for analysis: the genes with a total count below 10 across samples were
534 filtered out and the differential gene expression analysis was performed using DESeq version
535 1.40.2 integrated into EyeDVseq, comparing sham as control and vagotomy as the condition. The
536 resulting gene list was then filtered, with $|\log_2(\text{FoldChange})| > 0.5$ and pAdj values < 0.05 being
537 considered significant.

538 Single-cell mRNA sequencing and analysis

539 Live $CD11b^{+}CD45^{+}$ MPs were sorted from eyecups with and without laser, as described
540 above. Single cell mRNA sequencing (scRNAseq) libraries were prepared from sorted cells using
541 the Chromium Next GEM Single Cell 3' Library v3.1 and dual index TT kits (10X Genomics)
542 according to manufacturer's recommended protocol. Resulting libraries were sequenced on an
543 Illumina Novaseq 6000. The fastq files were processed using CellRanger v6.1.2 with default
544 options (alignment, count). The resulting expression matrices were merged and analyzed with
545 Seurat v4 (merging, QC filtering, normalization, PCA, clustering, and UMAP). The resulting
546 Seurat object was used to create an H5AD file that was loaded into cellxgene. Further analyses,
547 including differential gene expression analyses, and visualizations were performed in cellxgene

using the cellxgene_VIP plugin. Cells other than MPs (including rod photoreceptors and other retinal neurons) were excluded and then the remaining MPs were re-clustered. Differentially expressed genes were identified using the cellxgene Welch's t test, and the resulting gene lists were filtered with adjusted p-value < 0.05 and $|\log \text{Fold Change}| > 0.2$ considered significant. Processing scripts are available on request.

Statistical analysis

GraphPad Prism 10 was used for data analysis and graphic representation, unless otherwise stated (see above for details of the cohort study and RNA sequencing analyses). Data are presented as mean ± standard error of the mean (SEM). Differences between two groups were analyzed using an unpaired Mann-Whitney test and differences between multiple groups were analyzed using a one-way ANOVA followed by a Tukey's multiple comparisons test. The n and p-values are indicated in the figure legends.

References

Aldebert, G., Faillie, J. L., Hillaire-Buys, D., Mura, T., Carriere, I., Delcourt, C., Creuzot-Garcher, C., Villain, M., & Daien, V. (2018). Association of Anticholinergic Drug Use With Risk for Late Age-Related Macular Degeneration. *JAMA Ophthalmol*, *136*(7), 770-778. https://doi.org/10.1001/jamaophthalmol.2018.1719

Andersson, U., & Tracey, K. J. (2012). Neural reflexes in inflammation and immunity. *J Exp Med*, *209*(6), 1057-1068. https://doi.org/10.1084/jem.20120571

Baker, M. C., Nagy, D., Tamang, S., Horvath-Puho, E., & Sorensen, H. T. (2025). Vagotomy and the incidence of rheumatoid arthritis and osteoarthritis: a Danish register-based study. *Arthritis Res Ther*, *27*(1), 106. https://doi.org/10.1186/s13075-025-03567-y

Beguier, F., Housset, M., Roubeix, C., Augustin, S., Zagar, Y., Nous, C., Mathis, T., Eandi, C., Benchaboune, M., Drame-Maigne, A., Carpentier, W., Chardonnet, S., Touhami, S., Blot, G., Conart, J. B., Charles-Messance, H., Potey, A., Girmens, J. F., Paques, M., . . . Sennlaub, F. (2020). The 10q26 Risk Haplotype of Age-Related Macular Degeneration Aggravates Subretinal Inflammation by Impairing Monocyte Elimination. *Immunity*, *53*(2), 429-441 e428. https://doi.org/10.1016/j.immuni.2020.07.021

Bodin, F., McIntyre, K. M., Schwartz, J. E., McKinley, P. S., Cardetti, C., Shapiro, P. A., Gorenstein, E., & Sloan, R. P. (2017). The Association of Cigarette Smoking With High-Frequency Heart Rate Variability: An Ecological Momentary Assessment Study. *Psychosom Med*, *79*(9), 1045-1050. https://doi.org/10.1097/PSY.0000000000000507

Borovikova, L. V., Ivanova, S., Zhang, M., Yang, H., Botchkina, G. I., Watkins, L. R., Wang, H., Abumrad, N., Eaton, J. W., & Tracey, K. J. (2000). Vagus nerve stimulation attenuates the systemic inflammatory response to endotoxin. *Nature*, *405*(6785), 458-462. https://doi.org/10.1038/35013070

Calippe, B., Augustin, S., Beguier, F., Charles-Messance, H., Poupel, L., Conart, J. B., Hu, S. J., Lavalette, S., Fauvet, A., Rayes, J., Levy, O., Raoul, W., Fitting, C., Denefle, T., Pickering, M. C., Harris, C., Jorieux, S., Sullivan, P. M., Sahel, J. A., . . . Sennlaub, F. (2017). Complement Factor H Inhibits CD47-Mediated Resolution of Inflammation. *Immunity*, *46*(2), 261-272. https://doi.org/10.1016/j.immuni.2017.01.006

Carnevale, D., Perrotta, M., Pallante, F., Fardella, V., Iacobucci, R., Fardella, S., Carnevale, L., Carnevale, R., De Lucia, M., Cifelli, G., & Lembo, G. (2016). A cholinergic-sympathetic pathway primes immunity in hypertension and mediates brain-to-spleen communication. *Nat Commun*, *7*, 13035. https://doi.org/10.1038/ncomms13035

Chavan, S. S., Pavlov, V. A., & Tracey, K. J. (2017). Mechanisms and Therapeutic Relevance of Neuro-immune Communication. *Immunity*, *46*(6), 927-942. https://doi.org/10.1016/j.immuni.2017.06.008

Chen, H., Feng, Z., Min, L., Deng, W., Tan, M., Hong, J., Gong, Q., Zhang, D., Liu, H., & Hou, J. (2022). Vagus Nerve Stimulation Reduces Neuroinflammation Through Microglia Polarization Regulation to Improve Functional Recovery After Spinal Cord Injury. *Front Neurosci*, *16*, 813472. https://doi.org/10.3389/fnins.2022.813472

Chong, S. Z., Evrard, M., Devi, S., Chen, J., Lim, J. Y., See, P., Zhang, Y., Adrover, J. M., Lee, B., Tan, L., Li, J. L., Liong, K. H., Phua, C., Balachander, A., Boey, A., Liebl, D., Tan, S. M., Chan, J. K., Balabanian, K., . . . Ng, L. G. (2016). CXCR4 identifies transitional bone marrow premonocytes that replenish the mature monocyte pool for peripheral responses. *J Exp Med*, *213*(11), 2293-2314. https://doi.org/10.1084/jem.20160800

605 Cseh, B., Fernandez-Sauze, S., Grall, D., Schaub, S., Doma, E., & Van Obberghen-Schilling, E.
606 (2010). Autocrine fibronectin directs matrix assembly and crosstalk between cell-matrix
607 and cell-cell adhesion in vascular endothelial cells. *J Cell Sci*, *123*(Pt 22), 3989-3999.
608 https://doi.org/10.1242/jcs.073346
609 Fleckenstein, M., Keenan, T. D. L., Guymer, R. H., Chakravarthy, U., Schmitz-Valckenberg, S.,
610 Klaver, C. C., Wong, W. T., & Chew, E. Y. (2021). Age-related macular degeneration. *Nat*
611 *Rev Dis Primers*, *7*(1), 31. https://doi.org/10.1038/s41572-021-00265-2
612 Grunin, M., Hagbi-Levi, S., Rinsky, B., Smith, Y., & Chowers, I. (2016). Transcriptome Analysis
613 on Monocytes from Patients with Neovascular Age-Related Macular Degeneration. *Sci*
614 *Rep*, *6*, 29046. https://doi.org/10.1038/srep29046
615 Guillonneau, X., Eandi, C. M., Paques, M., Sahel, J. A., Sapieha, P., & Sennlaub, F. (2017). On
616 phagocytes and macular degeneration. *Prog Retin Eye Res*, *61*, 98-128.
617 https://doi.org/10.1016/j.preteyeres.2017.06.002
618 Hallak, J. A., Abbasi, A., Goldberg, R. A., Modi, Y., Zhao, C., Jing, Y., Chen, N., Mercer, D.,
619 Sahu, S., Alobaidi, A., Lopez, F. J., Luhrs, K., Waring, J. F., den Hollander, A. I., &
620 Smaoui, N. (2024). Janus Kinase Inhibitor Therapy and Risk of Age-Related Macular
621 Degeneration in Autoimmune Disease. *JAMA Ophthalmol*, *142*(8), 750-758.
622 https://doi.org/10.1001/jamaophthalmol.2024.2376
623 Huang, K., Schofield, C., Nguy, T., Dere, R., Wolowski, V., Siebourg-Polster, J., Dieckmann, A.,
624 Garweg, J. G., Chang, M., Honigberg, L., Hackney, J., & Indjeian, V. B. (2025).
625 Proteomics approach identifies aqueous humor biomarkers in retinal diseases. *Commun*
626 *Med (Lond)*, *5*(1), 134. https://doi.org/10.1038/s43856-025-00862-2
627 Koopman, F. A., Chavan, S. S., Miljko, S., Grazio, S., Sokolovic, S., Schuurman, P. R., Mehta, A.
628 D., Levine, Y. A., Faltys, M., Zitnik, R., Tracey, K. J., & Tak, P. P. (2016). Vagus nerve
629 stimulation inhibits cytokine production and attenuates disease severity in rheumatoid
630 arthritis. *Proc Natl Acad Sci U S A*, *113*(29), 8284-8289.
631 https://doi.org/10.1073/pnas.1605635113
632 Lad, E. M., Cousins, S. W., Van Arnam, J. S., & Proia, A. D. (2015). Abundance of infiltrating
633 CD163+ cells in the retina of postmortem eyes with dry and neovascular age-related
634 macular degeneration. *Graefes Arch Clin Exp Ophthalmol*, *253*(11), 1941-1945.
635 https://doi.org/10.1007/s00417-015-3094-z
636 Lagoo, J., Pappas, T. N., & Perez, A. (2014). A relic or still relevant: the narrowing role for
637 vagotomy in the treatment of peptic ulcer disease. *Am J Surg*, *207*(1), 120-126.
638 https://doi.org/10.1016/j.amjsurg.2013.02.012
639 Lechner, J., Chen, M., Hogg, R. E., Toth, L., Silvestri, G., Chakravarthy, U., & Xu, H. (2017).
640 Peripheral blood mononuclear cells from neovascular age-related macular degeneration
641 patients produce higher levels of chemokines CCL2 (MCP-1) and CXCL8 (IL-8). *J*
642 *Neuroinflammation*, *14*(1), 42. https://doi.org/10.1186/s12974-017-0820-y
643 Levy, O., Lavalette, S., Hu, S. J., Housset, M., Raoul, W., Eandi, C., Sahel, J. A., Sullivan, P. M.,
644 Guillonneau, X., & Sennlaub, F. (2015). APOE-isoforms control pathogenic subretinal
645 inflammation in age related macular degeneration. *J Neurosci*, *35*(40), 13568 –13576.
646 https://doi.org/10.1523/JNEUROSCI.2468-15.2015
647 McGuinness, M. B., Le, J., Mitchell, P., Gopinath, B., Cerin, E., Saksens, N. T. M., Schick, T.,
648 Hoyng, C. B., Guymer, R. H., & Finger, R. P. (2017). Physical Activity and Age-related
649 Macular Degeneration: A Systematic Literature Review and Meta-analysis. *Am J*
650 *Ophthalmol*, *180*, 29-38. https://doi.org/10.1016/j.ajo.2017.05.016

651 Miller, E. B., Karlen, S. J., Ronning, K. E., & Burns, M. E. (2021). Tracking distinct microglia
652 subpopulations with photoconvertible Dendra2 in vivo. *J Neuroinflammation*, *18*(1), 235.
653 https://doi.org/10.1186/s12974-021-02285-x
654 Molbech, C. R., Boegh, M. M., Nielsen, M. K., Subhi, Y., Liisborg, C., Roubeix, C., Sennlaub, F.,
655 Mehlsen, J., & Sorensen, T. L. (2025). Impaired Vagal Tone Function-Based Regulation
656 of Systemic Inflammation in Patients With Neovascular Age-Related Macular
657 Degeneration. *Invest Ophthalmol Vis Sci*, *66*(13), 16. https://doi.org/10.1167/iovs.66.13.16
658 Nahavandipour, A., Krogh Nielsen, M., Sorensen, T. L., & Subhi, Y. (2020). Systemic levels of
659 interleukin-6 in patients with age-related macular degeneration: a systematic review and
660 meta-analysis. *Acta Ophthalmol*, *98*(5), 434-444. https://doi.org/10.1111/aos.14402
661 Robbins, C. S., Chudnovskiy, A., Rauch, P. J., Figueiredo, J. L., Iwamoto, Y., Gorbatov, R.,
662 Etzrodt, M., Weber, G. F., Ueno, T., van Rooijen, N., Mulligan-Kehoe, M. J., Libby, P.,
663 Nahrendorf, M., Pittet, M. J., Weissleder, R., & Swirski, F. K. (2012). Extramedullary
664 hematopoiesis generates Ly-6C(high) monocytes that infiltrate atherosclerotic lesions.
665 *Circulation*, *125*(2), 364-374. https://doi.org/10.1161/CIRCULATIONAHA.111.061986
666 Rosas-Ballina, M., Ochani, M., Parrish, W. R., Ochani, K., Harris, Y. T., Huston, J. M., Chavan,
667 S., & Tracey, K. J. (2008). Splenic nerve is required for cholinergic antiinflammatory
668 pathway control of TNF in endotoxemia. *Proc Natl Acad Sci U S A*, *105*(31), 11008-11013.
669 https://doi.org/10.1073/pnas.0803237105
670 Roubeix, C., Nous, C., Augustin, S., Ronning, K. E., Mathis, T., Blond, F., Lagouge-Roussey, P.,
671 Crespo-Garcia, S., Sullivan, P. M., Gautier, E. L., Reichhart, N., Sahel, J. A., Burns, M. E.,
672 Paques, M., Sorensen, T. L., Strauss, O., Guillonneau, X., Delarasse, C., & Sennlaub, F.
673 (2024). Splenic monocytes drive pathogenic subretinal inflammation in age-related
674 macular degeneration. *J Neuroinflammation*, *21*(1), 22. https://doi.org/10.1186/s12974-
675 024-03011-z
676 Schmidt, M., Pedersen, L., & Sorensen, H. T. (2014). The Danish Civil Registration System as a
677 tool in epidemiology. *Eur J Epidemiol*, *29*(8), 541-549. https://doi.org/10.1007/s10654-
678 014-9930-3
679 Schmidt, M., Schmidt, S. A. J., Adelborg, K., Sundboll, J., Laugesen, K., Ehrenstein, V., &
680 Sorensen, H. T. (2019). The Danish health care system and epidemiological research: from
681 health care contacts to database records. *Clin Epidemiol*, *11*, 563-591.
682 https://doi.org/10.2147/CLEP.S179083
683 Sennlaub, F., Auvynet, C., Calippe, B., Lavalette, S., Poupel, L., Hu, S. J., Dominguez, E., Camelo,
684 S., Levy, O., Guyon, E., Saederup, N., Charo, I. F., Rooijen, N. V., Nandrot, E., Bourges,
685 J. L., Behar-Cohen, F., Sahel, J. A., Guillonneau, X., Raoul, W., & Combadiere, C. (2013).
686 CCR2(+) monocytes infiltrate atrophic lesions in age-related macular disease and mediate
687 photoreceptor degeneration in experimental subretinal inflammation in Cx3cr1 deficient
688 mice. *EMBO Mol Med*, *5*(11), 1775-1793. https://doi.org/10.1002/emmm.201302692
689 Shinkai, Y., Rathbun, G., Lam, K. P., Oltz, E. M., Stewart, V., Mendelsohn, M., Charron, J., Datta,
690 M., Young, F., Stall, A. M., & et al. (1992). RAG-2-deficient mice lack mature
691 lymphocytes owing to inability to initiate V(D)J rearrangement. *Cell*, *68*(5), 855-867.
692 https://doi.org/10.1016/0092-8674(92)90029-c
693 Svensson, E., Horvath-Puho, E., Thomsen, R. W., Djurhuus, J. C., Pedersen, L., Borghammer, P.,
694 & Sorensen, H. T. (2015). Vagotomy and subsequent risk of Parkinson's disease. *Ann
695 Neurol*, *78*(4), 522-529. https://doi.org/10.1002/ana.24448

Swirski, F. K., Nahrendorf, M., Etzrodt, M., Wildgruber, M., Cortez-Retamozo, V., Panizzi, P., Figueiredo, J. L., Kohler, R. H., Chudnovskiy, A., Waterman, P., Aikawa, E., Mempel, T. R., Libby, P., Weissleder, R., & Pittet, M. J. (2009). Identification of splenic reservoir monocytes and their deployment to inflammatory sites. *Science*, *325*(5940), 612-616. https://doi.org/10.1126/science.1175202

VanderWeele, T. J., & Ding, P. (2017). Sensitivity Analysis in Observational Research: Introducing the E-Value. *Ann Intern Med*, *167*(4), 268-274. https://doi.org/10.7326/M16-2607

Yu, C., Roubeix, C., Sennlaub, F., & Saban, D. R. (2020). Microglia versus Monocytes: Distinct Roles in Degenerative Diseases of the Retina. *Trends Neurosci*, *43*(6), 433-449. https://doi.org/10.1016/j.tins.2020.03.012

Zhang, L., Liu, Y., Wang, S., Long, L., Zang, Q., Ma, J., Yu, L., & Jia, G. (2021). Vagus nerve stimulation mediates microglia M1/2 polarization via inhibition of TLR4 pathway after ischemic stroke. *Biochem Biophys Res Commun*, *577*, 71-79. https://doi.org/10.1016/j.bbrc.2021.09.004

Zhang, X., Lei, B., Yuan, Y., Zhang, L., Hu, L., Jin, S., Kang, B., Liao, X., Sun, W., Xu, F., Zhong, Y., Hu, J., & Qi, H. (2020). Brain control of humoral immune responses amenable to behavioural modulation. *Nature*, *581*(7807), 204-208. https://doi.org/10.1038/s41586-020-2235-7

Acknowledgements

We would like to thank Daniela Carnevale for initial training in performing cervical vagotomies in mice. We gratefully acknowledge the Cordelier Histology, Imaging, Cytometry and Spatialomics (CHICS) core facility (Centre de Recherche des Cordeliers, U1138, INSERM, Sorbonne Université, Université Paris Cité, 75006 Paris, France) for histological preparation and multiplex immunohistochemistry. This work benefited from equipment and services from the iGenSeq core facility at ICM. We would also like to thank the Imaging Core Facility, the Phénotypage Cellulaire et Tissulaire platform, and the animal facility of the Institut de la Vision.

This work was supported by the Agence Nationale de la Recherche (ANR, France: IHU FOReSIGHT [ANR-18-IAHU-0001], ANR Osaging [ANR-180CE14-0311-02], and ANR KEVINplus [ANR-22-CE14-0015-01]), a Berthe Fouassier Fondation de France post-doctoral fellowship, the MSCA Seal of Excellence program at Sorbonne University (VagalToneAMD), Retina France, Fondation Valentin Hauÿ, the Carnot Institute (France), and the Institut National de la Santé et de la Recherche Médicale (INSERM, France).

731 **Table 1.** Incidence rates and hazard ratios of age-related macular degeneration for
732 vagotomy patients surviving 10 years after vagotomy and their comparison cohort. AMD = age-
733 related macular degeneration; COPD = chronic obstructive pulmonary disease; CCI = Charlson
734 comorbidity index.

	No. of AMD	Incidence Rate (per 1000 person-years at risk) (95% CI)	Hazard ratio controlled for age and gender by design	Adjusted for age, gender, and COPD	Adjusted for age, gender, and obesity-related diseases	Adjusted for age, gender, and hypertension	Adjusted for age, gender, and CCI	Adjusted for age, gender, COPD, obesity-related diseases, hypertension and CCI
Comparison cohort	3070	2.40 (2.31-2.48)						
All vagotomy	360	3.00 (2.69-3.31)	1.37 (1.22-1.55)	1.36 (1.21-1.53)	1.37 (1.22-1.54)	1.37 (1.22-1.55)	1.37 (1.21-1.54)	1.36 (1.21-1.53)
Comparison cohort	1400	2.85 (2.70-3.00)						
Truncal vagotomy	170	3.85 (3.29-4.44)	1.47 (1.23-1.74)	1.46 (1.23-1.73)	1.46 (1.23-1.74)	1.47 (1.24-1.74)	1.46 (1.23-1.73)	1.45 (1.22-1.73)
Comparison cohort	1550	2.09 (1.99-2.19)						
Superselective vagotomy	180	2.47 (2.12-2.85)	1.31 (1.11-1.55)	1.30 (1.10-1.53)	1.31 (1.11-1.55)	1.31 (1.11-1.55)	1.30 (1.10-1.54)	1.29 (1.09-1.53)

735

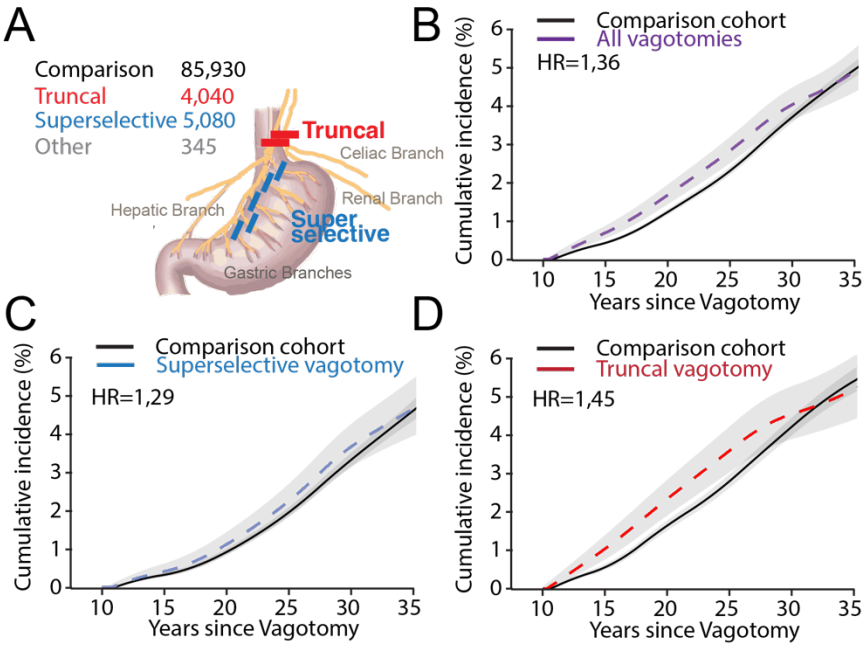

Figure 1. Vagotomy is associated with increased incidence of AMD.

(A) Study cohorts included all patients in Denmark who underwent vagotomy between 1977 and 1995 with ≥10 years follow-up (n=9,465), subdivided into truncal vagotomy (TV, n=4,040), superselective vagotomy (SSV, n=5,080), and unspecified type (n=345). Each patient was matched to 10 individuals from the general population (n=85,930) by exact birth year and sex using the Civil Registration System. The schematic illustrates that TV denervates abdominal organs including the celiac branch that innervates the spleen, whereas SSV primarily targets gastric branches and spares extra-gastric innervation.

(B) Cumulative incidence of AMD in all vagotomized patients compared to their matched population cohort.

(C) Cumulative incidence of AMD in patients with superselective vagotomy compared to their matched cohort.

(D) Cumulative incidence of AMD in patients with truncal vagotomy compared to their matched cohort.

Follow-up began 10 years after index date as the Civil Registry was only available from 1986; curves were estimated using Kaplan–Meier analysis treating death as a competing risk and smoothed for visualization using splines. Hazard ratios (HR) were obtained from Cox regression adjusted for age, sex, COPD, obesity-related diseases, hypertension, and Charlson Comorbidity Index categories (full details in Table 1 and Supplemental Tables 1–3).

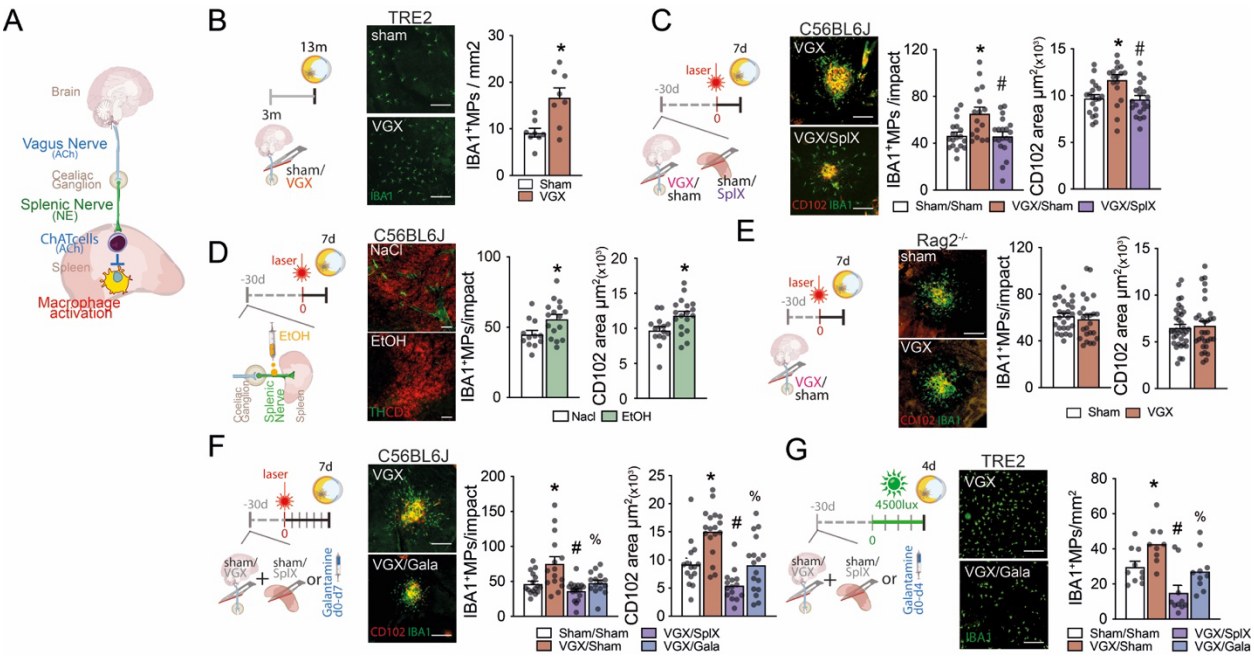

Figure 2. Vagotomy promotes inflammation and exacerbates disease severity in mouse models of AMD in a spleen-dependent manner.

(A) Schematic of the parasympathetic vagus–spleen axis: Acetylcholine from vagal efferents activate the splenic nerve at the coeliac ganglion, increasing splenic norepinephrine and driving ChAT^{+} T cell–derived acetylcholine that tonically restrains mononuclear phagocytes (MPs).

(B) Representative images and quantification of subretinal IBA1^{+} MPs on IBA1-stained RPE/choroidal flatmounts from TRE2 mice subjected to left cervical truncal vagotomy at 3 months and analyzed at 13 months (n=8 per group; Mann-Whitney test *p=0.0148).

(C) Laser-induced choroidal neovascularization (CNV) model in 3-month-old male C57BL/6J mice: vagotomy with or without splenectomy performed 1 month before laser (at 2 months old); quantification of subretinal IBA1^{+} MP counts and CD102^{+} CNV area on IBA1/CD102 double-stained RPE/choroidal flatmounts 7 days after laser injury (n= 16-20 per group; one-way ANOVA/Tukey: IBA1 Sham/Sham versus VGX/Sham *p=0.0057, VGX/Sham versus VGX/SplX #p=0.0034, Sham/Sham versus VGX/SplX not significant (ns); CD102 Sham/Sham versus VGX/Sham *p=0.0123, VGX/Sham versus VGX/SplX #p=0.0068, Sham/Sham versus VGX/SplX ns).

(D) Splenic denervation in 2-month-old male C57BL/6J mice by ethanol application at the splenic hiatus: (left) verification by loss of tyrosine-hydroxylase (TH, green)(co-stained for CD3,

776 magenta, and DAPI, blue) immunostaining on spleen sections; (right) quantification of subretinal
777 IBA1^{+} MP counts and CD102^{+} CNV area on IBA1/CD102 double-stained RPE/choroidal
778 flatmounts 7 days after laser injury (laser 1 month post-surgery)(n= 12-18 per group; Mann-
779 Whitney: IBA1 *p=0.0284; CD102 *p=0.0118).
780 (E) Laser model in 2-month-old male Rag2$^{-/-}$ mice (lacking mature lymphocytes including
781 ChAT^{+} T cells): quantification of subretinal IBA1^{+} MPs and CD102^{+} CNV area on IBA1/CD102
782 double-stained RPE/choroidal flatmounts 7 days after laser injury (n= 24-26 per group; Mann-
783 Whitney: IBA1 and CD102 not statistically significant).
784 (F) Daily intraperitoneal galantamine (an acetylcholinesterase inhibitor, 4 mg/kg) initiated
785 after laser in previously vagotomized 3-month-old male C57BL/6J mice: quantification of IBA1^{+}
786 MP counts and CD102^{+} CNV area on IBA1/CD102 double-stained RPE/choroidal flatmounts 7
787 days after laser injury (n= 15-17 per group; one-way ANOVA/Tukey: IBA1 Sham/Sham versus
788 VGX/Sham *p=0.005, VGX/Sham versus VGX/SplX #p<0.001, VGX/Sham versus VGX/Gala
789 %p=0.0093; CD102 Sham/Sham versus VGX/Sham *p=0.0009, VGX/Sham versus VGX/SplX
790 #p<0.0001, VGX/Sham versus VGX/Gala %p=0.0004).
791 (G) Bright-light challenge calibrated to induce subretinal MP infiltration in TRE2 but not
792 controls; quantification of IBA1^{+} MPs on IBA1-stained RPE flatmounts from 3-month-old male
793 TRE2 mice after 4 days of light exposure, one month after sham or vagotomy with or without
794 splenectomy or daily galantamine (4 mg/kg)(n=9-10 per group; one-way ANOVA/Tukey:
795 Sham/Sham versus VGX/Sham *p=0.0344, VGX/Sham versus VGX/SplX #p<0.0001,
796 VGX/Sham versus VGX/Gala %p=0.0285).
797 Statistics: data are represented as mean ± SEM, Mann-Whitney test (two-group
798 comparisons) or one-way ANOVA with Tukey's test (multiple comparisons) as indicated;
799 replicates represent quantifications of eyes or plasma samples from different mice (C57BL/6Js
800 were all males, TRE2 were males and females) from at least three independent cages/experiments.
801 ChAT: choline acetyltransferase; TRE2: targeted-replacement mice expressing human APOE2;
802 MP: mononuclear phagocyte; CNV: choroidal neovascularization. Scale bars: 20µm

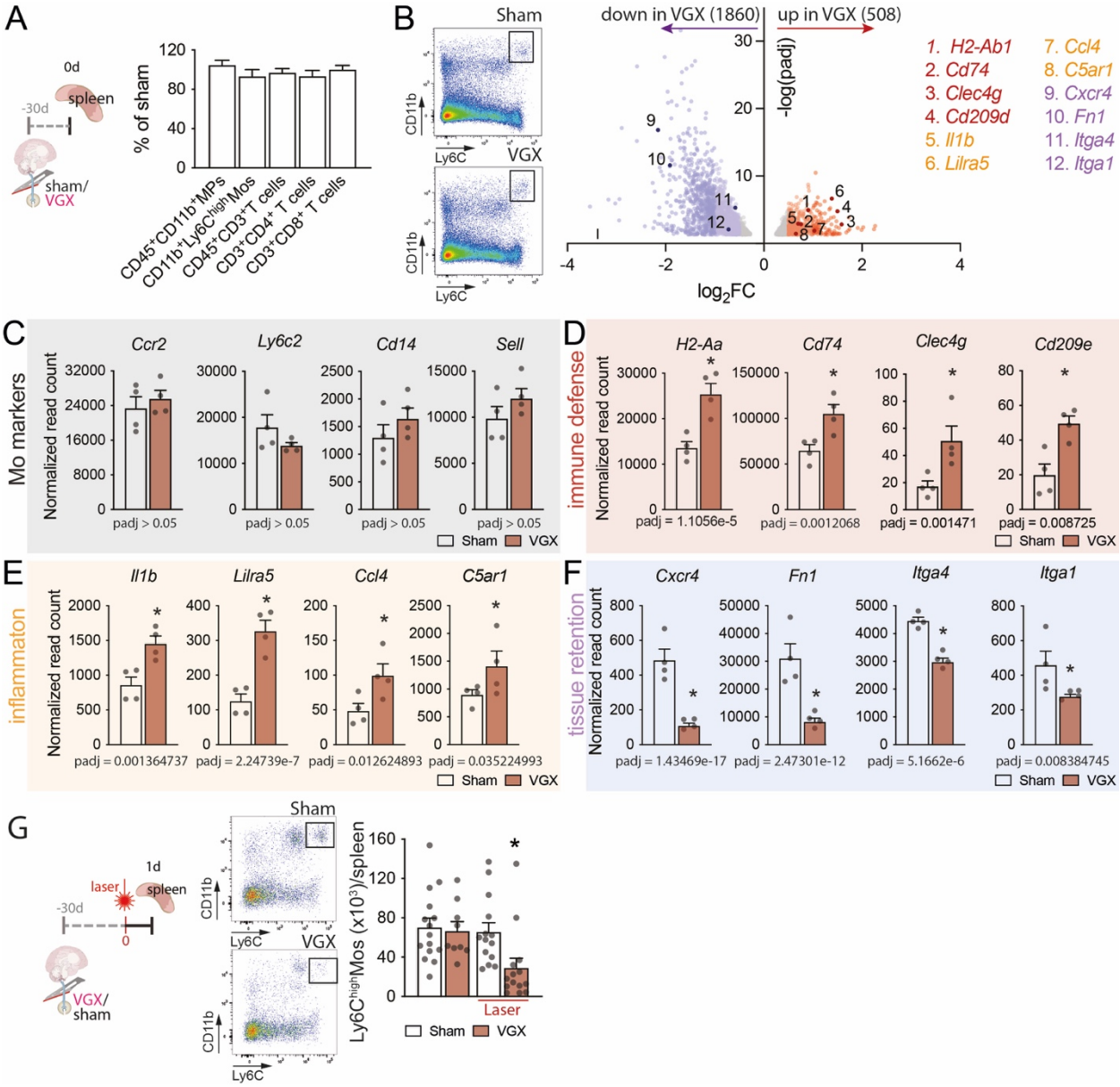

Figure 3. Loss of vagal tone reshapes the splenic monocyte transcriptome and drives their mobilization.

(A) Flow cytometric quantification of splenic CD45$^+$CD11b$^+$ MPs, CD45$^+$CD11b$^+$Ly6C^{high} monocytes (Mos), CD4$^+$ T cells, and CD8$^+$ T cells from 3-month-old male mice 30 days after vagotomy (VGX) or sham surgery, expressed as percentage of sham (see Supplemental Fig. 1 for comparisons between sham and VGX).

B) Bulk RNA sequencing of FACS-sorted CD45$^+$CD11b$^+$Ly6G^{neg}Ly6C^{high} splenic Mos: (left) representative flow plots; (right) volcano plot showing downregulated (n=1860) and upregulated (n=508) genes in VGX versus sham (right), with selected genes highlighted.

(C–F) Normalized read counts of selected genes: (C) classical monocyte markers (*Ccr2*, *Ly6c2*, *Cd14*, *Sell*); (D) immune defense–associated genes (*H2-Aa*, *Cd74*, *Clec4g*, *Cd209e*); (E) inflammatory genes (*Il1b*, *Lilra5*, *Ccl4*, *C5ar1*); (F) tissue retention–associated genes (*Cxcr4*, *Fn1*, *Itga4*, *Itga1*). Adjusted p values are indicated in the figure.

(G) Experimental schematic of vagotomy/sham followed by laser injury or no injury 30 days later, with analysis at day 1 (left) and representative flow cytometric plots and quantification of splenic Ly6C^{high} Mos from sham and VGX mice with or without laser (right, n=9-15 per group; Mann-Whitney: Laser Sham versus VGX *p=0.001; no laser Sham versus VGX not statistically significant).

Statistics: (G) data are represented as mean ± SEM, Mann-Whitney test (two-group comparisons); (B-F) see methods for RNAseq analysis details; replicates represent spleens from different mice (all males). MP: mononuclear phagocyte; Mo: monocyte; VGX: vagotomy.

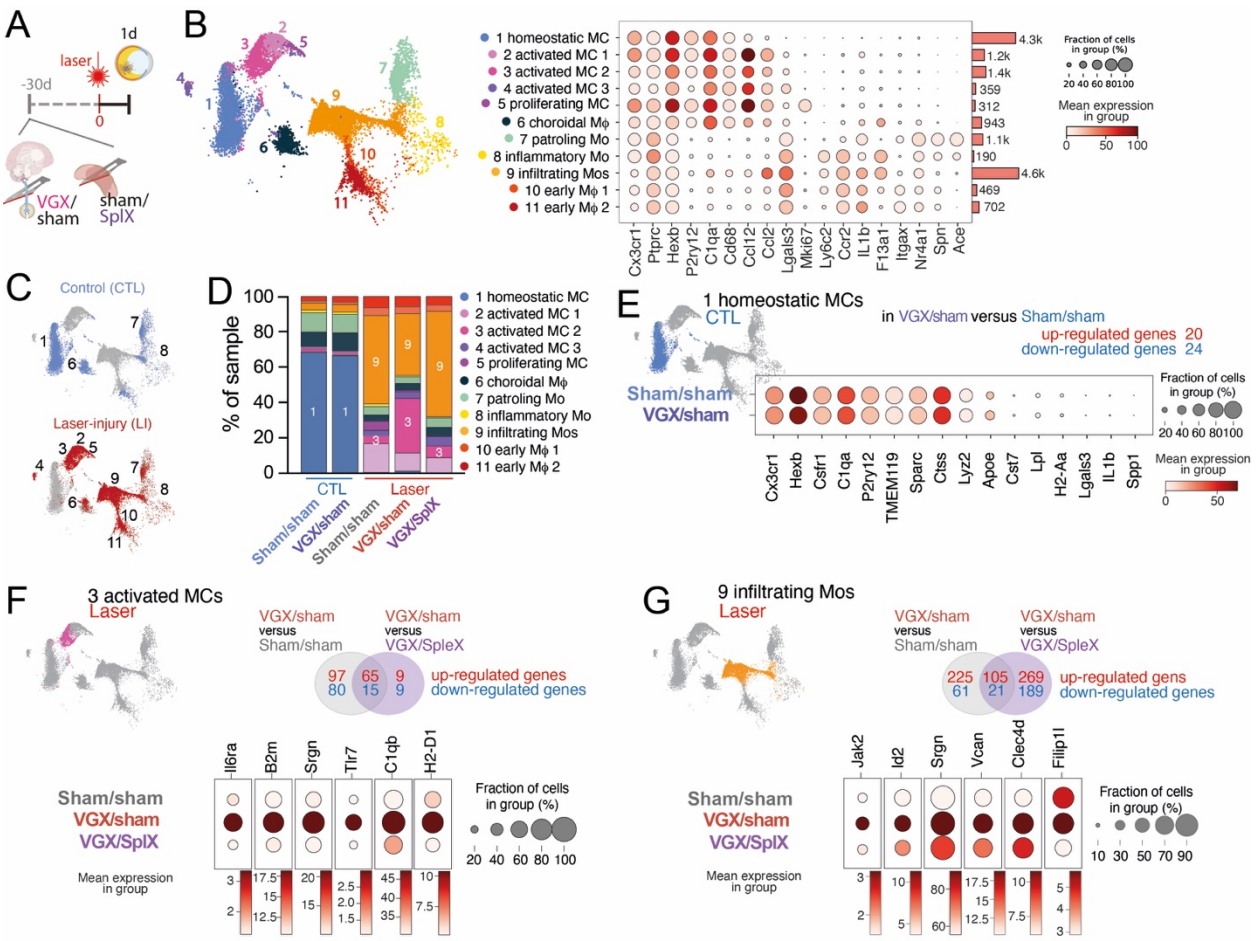

Figure 4. Vagotomy induces transcriptional reprogramming of infiltrating monocytes and activated microglia in the retina in a spleen-dependent manner.

(A) CD45^{+}CD11b^{+} cells were FACS-sorted from posterior eye segments of mice 1 month after sham or vagotomy (VGX), and from mice 1 day after laser injury that had undergone sham, VGX, or VGX with splenectomy (VGX+SPLX) one month prior.

(B) UMAP projection of myeloid cell clusters (left) and dot plot showing expression of representative marker genes (right).

(C) Distribution of cells between control (non-lasered, CTL) and lasered samples.

(D) Relative proportions of each cluster across experimental conditions.

(E) Expression of representative homeostatic and activated microglia genes in the homeostatic microglia cluster from non-lasered sham and VGX samples.

(F) Differential gene expression analysis of cluster 3 (activated MC2) between surgery conditions (top), with representative genes shown as dot plots (bottom).

839 (G) Differential gene expression analysis of cluster 9 (infiltrating monocytes, Mos)
840 between surgery conditions (top), with representative genes shown as dot plots (bottom).
841 VGX: vagotomy; SplX: splenectomy; CTL: control; LI: laser injury.